PCCP

COMMUNICATION

View Article Online
View Journal | View Issue

Cite this: *Phys. Chem. Chem. Phys.*, 2022, **24**, 11491

Received 21st January 2022,
Accepted 25th April 2022

DOI: 10.1039/d2cp00340f

rsc.li/pccp

Connection of Ru nanoparticles with rich defects enables the enhanced electrochemical reduction of nitrogen†

Xingrui Tang,‡[a] Xiuquan Tian,‡[a] Li Zhou,[a] Fan Yang,[a] Rong He,[a] Xu Zhao *[b] and Wenkun Zhu *[a]

The electrochemical reduction of N_2 into NH_3 under ambient conditions is an attractive topic in the chemical industry, but the chemical inertness of N_2 and the competing hydrogen evolution reaction hamper the activity and selectivity of this reaction. Herein, we connected Ru nanocrystals through a facile annealing process, which constructed intraparticle grain boundaries and stacking faults in the connection regions to enhance the N_2 reduction reaction. The connected Ru nanoparticles exhibited an enhanced yield rate and faradaic efficiency for NH_3 production. At −0.1 V *versus* RHE, the connected Ru nanoparticles exhibited a maximum yield rate of 29.3 μg cm^{-2} h^{-1} (148.0 μg mg_{cat}^{-1} h^{-1}) for NH_3 production with a faradaic efficiency of 7.0%. Mechanistic study revealed that the promotion of the electrochemical reduction of N_2 over connected Ru nanoparticles could be attributed to the decreased work function and facilitated electron transfer, which originated from the abundant defects in the connection region.

As an important chemical in agricultural, plastic, and textile industries, ammonia (NH_3) has played a vital role in economic development.[1–3] Moreover, NH_3 can serve as a stable hydrogen (H_2) carrier, which acts as a crucial intermediate in clean energy conversion. Although the air contains 78% nitrogen, the highly stable triple bonds in N_2 exhibit a bond energy as high as 940 kJ mol^{-1}, resulting in a large energy barrier to activate the inert N_2.[4–6] The typical industrial process for the direct synthesis of NH_3 from N_2 is the Haber–Bosch process, which proceeds at relatively high temperature and pressure (150–350 atm, 350–550 °C) with a large consumption of H_2. Both the harsh reaction conditions and the H_2 source originate from fossil fuels, accounting for 1–2% of the total global energy consumption and a large amount of CO_2 emission.[7–9] As such, researchers are devoted to searching for an alternative and sustainable approach for NH_3 synthesis. Notably, the electrochemical reduction of N_2 has been proposed as an ideal process to convert electricity for NH_3 synthesis, where the electricity can be obtained from intermittent renewable energy, such as solar and wind energy.[10–12] The electrochemical reduction of N_2 can occur at room temperature with facile control of the reaction kinetics by manipulating the applied potentials. Such processes are generally operated in aqueous electrolytes using water as a hydrogen precursor. During the electrochemical reduction of N_2, the chemical inertness of N_2 compared to that of water commonly leads to the overwhelming hydrogen evolution reaction (HER), which always consumes the electrons in the cathode and decreases the faradaic efficiency (FE).[13–16] As a result, the development of electrocatalysts with efficiently promoted activation of the N≡N triple bonds is highly desired to boost their catalytic activity for the electrochemical reduction of N_2.

Recently, a variety of materials have been demonstrated as active catalysts for this reaction, such as Au nanocrystals, Ru nanocrystals, doped carbon materials, and metal single atoms.[17–20] Typically, Ru-based catalysts represent a class of highly efficient catalysts for the electrochemical reduction of N_2. A theoretical study reported that Ru-based catalysts possessed an active site (namely the B5 site) on which the N_2 cleavage process only required a low activation energy of 0.5 eV.[21,22] In this regard, several Ru-containing nanostructures have been constructed as electrocatalysts for electrocatalytic N_2 reduction. For example, Zeng and co-workers demonstrated that Ru single atoms on nitrogen-doped carbon achieved a record-high yield rate of 120.9 μg_{NH3} mg_{cat}^{-1} h^{-1} at −0.2 V with

[a] *State Key Laboratory of Environment-friendly Energy Materials, National Co-innovation Center for Nuclear Waste Disposal and Environmental Safety, Sichuan Co-Innovation Center for New Energetic Materials, Nuclear Waste and Environmental Safety Key Laboratory of Defense, School of National Defence Science & Technology, Southwest University of Science and Technology, Mianyang, 621010, Sichuan, China. E-mail: zhuwenkun@swust.edu.cn*

[b] *Key Laboratory of Material Chemistry for Energy Conversion and Storage (Ministry of Education), Hubei Key Laboratory of Material Chemistry and Service Failure, School of Chemistry and Chemical Engineering, Huazhong University of Science and Technology, Wuhan, Hubei, 430074, P. R. China. E-mail: zhaoxu91@hust.edu.cn*

† Electronic supplementary information (ESI) available. See DOI: https://doi.org/10.1039/d2cp00340f

‡ These authors contributed equally to this work.

a 2.1-fold higher FE than that of Ru nanoparticles for N_2 electrochemical reduction.[23] Moreover, Sun and co-workers proved that Ru_2P nanoparticles on reduced graphene oxide exhibited a high NH_3 yield of 32.8 μg h^{-1} mg_{cat}^{-1} and a high FE of 13.04% at −0.05 V.[24] For these metal-based electrocatalysts, defect structures might also have an important influence on the catalytic performance.[25] For instance, Kanan and co-workers have proved that the density of grain boundaries in Au nanoparticles could be responsible for the CO_2 reduction activity.[26] For N_2 electrochemical reduction, Au sub-nanoclusters have been demonstrated to exhibit much enhanced NH_3 yield and FE compared to those of Au nanoparticles.[27] Specifically, unsaturated metal atoms, such as the edge atoms of the nanoparticles, tend to migrate to neighboring sites, which might induce the conjunction of nanoparticles with the existence of grain boundaries and/or other defects and thus lead to altered catalytic performance. Therefore, the rational construction of defect structures of metal-based nanocrystals is a potential pathway to develop highly active electrocatalysts for the electrochemical reduction of N_2.

Herein, we connected Ru nanocrystals to construct intraparticle grain boundaries and stacking faults for an enhanced N_2 reduction reaction. Through a facile annealing process, the dispersed Ru nanocrystals were connected with each other to form wavy nanowires. These nanowires possessed abundant defects in conjunction regions. For the electrochemical reduction of N_2, these connected Ru nanoparticles showed a yield rate of 29.3 μg cm^{-2} h^{-1} (148.0 μg mg_{cat}^{-1} h^{-1}) for NH_3 production at −0.1 V *versus* RHE, which was 5.6-fold larger higher that of dispersed Ru nanoparticles. Moreover, the faradaic efficiency for NH_3 production over connected Ru nanoparticles was 3.7-times higher than that of pristine Ru nanoparticles. Further mechanistic study revealed that the abundant defects in connected Ru nanoparticles could decrease the work function of Ru catalysts, giving rise to facilitated electron transfer and thus promoting their activity for the electrochemical reduction of N_2.

To begin with, the dispersed Ru nanoparticles were hydrothermally synthesized using $RuCl_3$ as the precursor, $NaBH_4$ as the reductant, and poly(vinyl pyrrolidone) (PVP) as the capping agent. As shown in the transmission electron microscopy (TEM) image, these Ru nanoparticles were highly crystalline with an average size of 6.5 nm without connecting with each other (Fig. S1 and S2, ESI†). Fig. S3 (ESI†) shows the high-resolution TEM (HRTEM) image of dispersed Ru nanoparticles, illustrating their defect-free nature. The Ru nanoparticles were then connected with each other after a subsequent annealing process at 550 °C in N_2 atmosphere. As shown in Fig. 1a, the Ru nanoparticles were connected and generated wavy nanowires. Fig. 1b and c show the HRTEM images of the connected Ru nanoparticles. The parallel fringes with interplanar spacings of 0.21 nm were ascribed to the (101) facets of the *hcp* Ru phase. In Fig. 1b, a distinct grain boundary is clearly recorded in the kinked region of the connected Ru nanoparticles. The grain boundaries and stacking faults are marked in Fig. 1b and c. Obviously, the dark fringes in Fig. 1c demonstrate the existence of stacking faults in the twisted region of the connected Ru

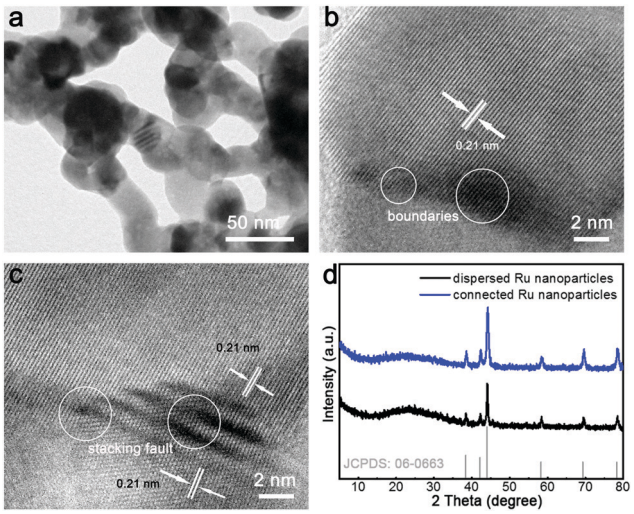

Fig. 1 (a) TEM images of connected Ru nanoparticles. (b and c) HRTEM images of connected Ru nanoparticles in different regions. (d) XRD patterns of dispersed Ru nanoparticles and connected Ru nanoparticles.

nanoparticles. These results indicate that various defects were generated along with the connection process of Ru nanoparticles. Fig. S4 (ESI†) shows that the Ru nanoparticles increased the boundaries and stacking faults, which were obtained by the increased annealing temperatures. Fig. 1d shows the X-ray diffraction (XRD) patterns of the dispersed Ru nanoparticles and connected Ru nanoparticles. All the peaks were indexed to *hcp* Ru (JCPDS No. 06-0663) without any shift. Moreover, the X-ray photoelectron spectroscopy (XPS) peaks of both the dispersed Ru nanoparticles and connected Ru nanoparticles correspond to zero-valent Ru (Fig. S5, ESI†), further verifying their metallic nature.[28–31]

To examine their electrochemical performance for N_2 electrochemical reduction, the dispersed Ru nanoparticles and connected Ru nanoparticles were uniformly dispersed on the electrode to prepare the working electrode. The concentration of ammonia was determined by the indophenol blue method, which showed a good linear fitting (Fig. S6, ESI†). Fig. 2a shows the geometric current density (j) of the connected Ru nanoparticles and dispersed Ru nanoparticles, while the corresponding LSV curves are shown in Fig. S7 (ESI†). The connected Ru nanoparticles exhibited higher currents than those of dispersed Ru at the applied potentials, which was attributed to the rich defects in the linked region of the Ru nanoparticles. Moreover, the yield rates for NH_3 production over connected Ru nanoparticles were remarkably higher than those over dispersed Ru nanoparticles at all of the applied potentials (Fig. 2b). The detailed yield rates and FE at different potentials in N_2-saturated electrolyte are collated in Table S1 (ESI†). Specifically, the yield rate for NH_3 production over connected Ru nanoparticles reached 29.3 μg cm^{-2} h^{-1} (148.0 μg mg_{cat}^{-1} h^{-1}) at −0.1 V *versus* RHE, which was 5.6-fold higher than that over dispersed Ru nanoparticles. Notably, such a high value of yield rate was also competitive with recently reported electrocatalysts for N_2 electrochemical

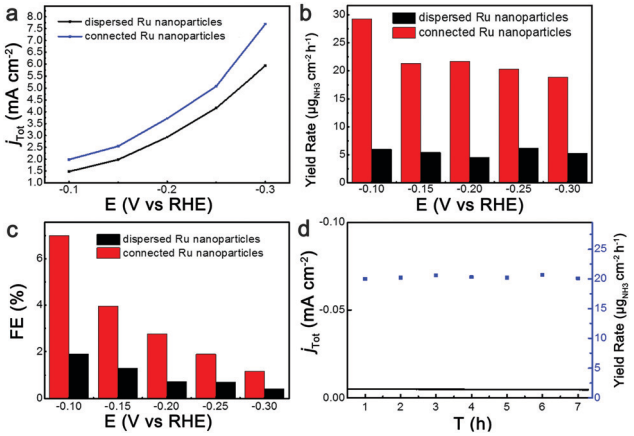

Fig. 2 (a) Total current densities for NH_3 production. (b) Yield rate and (c) faradaic efficiency for NH_3 production at different potentials over dispersed Ru nanoparticles and connected Ru nanoparticles. (d) The current density and yield rate for NH_3 production during a 7 h durability test at −0.1 V *versus* RHE over connected Ru nanoparticles.

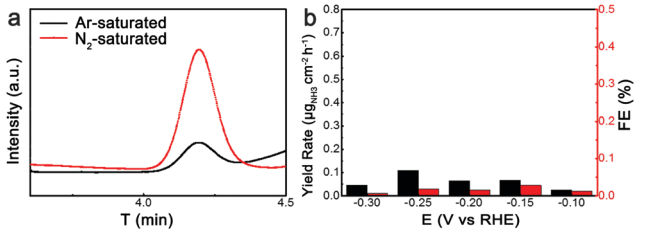

Fig. 3 (a) The NH^{4+} ion chromatography tests of the electrolyte after the catalytic reaction over connected Ru nanoparticles in Ar-saturated and N_2-saturated electrolytes. (b) Yield rate and FE of NH_3 production at different potentials over connected Ru nanoparticles in Ar-saturated electrolyte.

reduction (Table S2, ESI†).[32–38] Meanwhile, as shown in Fig. S8 (ESI†), the yield rate of NH_3 only exhibited slight decrease over connected Ru nanoparticles treated with PVP solution, demonstrating that PVP would have little effect on NH_3 production. Besides, to exclude the impacts of nitrate ions in the electrolyte, we have tested the nitrate ion concentration of the electrolyte using a UV spectrophotometer. The concentration of nitrate was determined by the absorbance at 220 nm minus twice the absorbance at 275 nm. The nitrate ion concentration in solution was below the detection limit. Furthermore, the faradaic efficiency analysis shown in Fig. S9 (ESI†) indicates that the products were mainly H_2 and NH_3, and no other substances were produced during the experiment.

The connection of Ru nanoparticles could also alter their selectivity for N_2 electrochemical reduction. Fig. 2c shows the FE for NH_3 production at the applied potentials. At −0.1 V *versus* RHE, the FE of the connected Ru nanoparticles reached 7.0%, which was higher than the 1.9% of the dispersed Ru nanoparticles. Under the other potentials, the connected Ru nanoparticles showed obvious outperformance in terms of the FE for NH_3 production compared to the dispersed Ru nanoparticles. Meanwhile, with increase in potential, the FE for NH_3 production of the two catalysts exhibited a dramatic decrease, which could be ascribed to the largely increased hydrogen evolution. Fig. 2d shows the stability test of the connected Ru nanoparticles under a constant potential of −0.1 V *versus* RHE. The connected Ru nanoparticles exhibited total current density without any obvious decay during the 7 h test. Meanwhile, the yield rate for NH_3 production over connected Ru nanoparticles was kept steady, further demonstrating the stability of the connected Ru nanoparticles.

To further verify the origin of NH_3 production over these Ru nanoparticles during the N_2 electrochemical reduction process, we performed control experiments in Ar-saturated and N_2-saturated electrolytes. The NH_4^+ ion chromatography tests of the electrolytes after catalytic reaction over the connected Ru nanoparticles in Ar-saturated and N_2-saturated electrolytes are collated in Fig. 3a. The signal obtained under the Ar-saturated condition over the connected Ru nanoparticles was relatively weak, indicating that the connected Ru nanoparticles hardly produced NH_3 without the presence of N_2. In contrast, a sharp peak corresponding to NH_4^+ ions emerged in the N_2-saturated electrolyte (Fig. S10, ESI†), demonstrating that the detected NH_3 mainly originated from the nitrogen source of N_2. Besides, when the reaction proceeded in an Ar-saturated electrolyte for 1 h over the connected Ru nanoparticles, the yield rate and FE of NH_3 production were below 0.15 μg cm^{-2} h^{-1} and 0.1%, respectively (Fig. 3b). Such performance was much poorer than that obtained in the N_2-saturated electrolyte, further demonstrating the lack of catalytic activity for NH_3 production in the absence of N_2. Moreover, we have also tested the open-circuit potential under nitrogen and argon atmospheres, where the influence of impurities in the atmosphere was further excluded (Fig. S11, ESI†). As such, for these Ru catalysts, NH_3 production is mainly derived from N_2 electrochemical reduction rather than the impurities present during the preparation and measurement of the catalysts.

The intrinsic cause of the high catalytic performance of connected Ru nanoparticles for NH_3 production was further explored. Fig. 4a shows the difference of charging current densities plotted against scan rate over the connected Ru nanoparticles and dispersed Ru nanoparticles, which was obtained by applying cyclic voltammetry (CV) ranging from 0.45 V to 0.35 V *versus* RHE at scan rates of 20, 40, 60, 80, and 100 mV s^{-1} at room temperature (Fig. S12, ESI†). The slope of the linear fit was twice the double-layer capacitance (C_{dl}) values. Specifically, the C_{dl} value of connected Ru nanoparticles was calculated to be 12.5 mF cm^{-2}, which was larger than the 9.1 mF cm^{-2} of the dispersed Ru nanoparticles. Given that the C_{dl} values were positively correlated with the electrochemical active surface area, the increased C_{dl} value of connected Ru nanoparticles suggested that the connection of Ru nanoparticles could lead to increased active sites for catalysis. The increased active sites of connected Ru could be ascribed to the presence of defects in the connection regions. Besides, we normalized the yield rate of NH_3 production at different potentials based on the C_{dl} values, which indicated the intrinsic activity excluding the influence of the number of active sites (Fig. 4b). At all of the

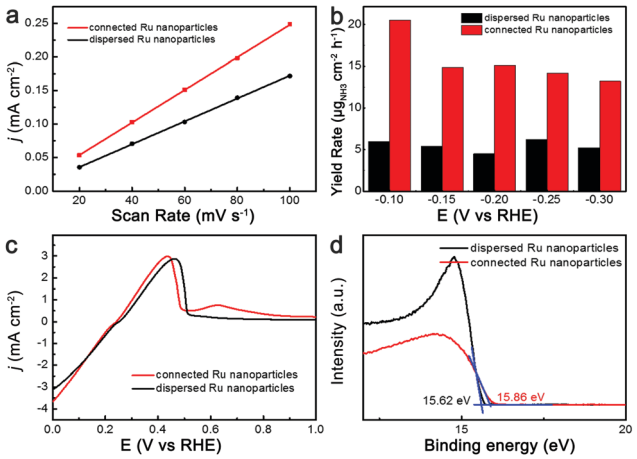

Fig. 4 (a) The differences of current density as a function of scan rate over dispersed Ru nanoparticles and connected Ru nanoparticles. (b) Normalized yield rate of NH_3 production at different potentials over dispersed Ru nanoparticles and connected Ru nanoparticles. (c) Cu-UPD stripping curves over dispersed Ru nanoparticles and connected Ru nanoparticles. (d) UPS spectra of dispersed Ru nanoparticles and connected Ru nanoparticles.

applied potentials, the normalized yield rate of NH_3 over the connected Ru nanoparticles showed an obvious enhancement compared to that on the dispersed Ru nanoparticles, indicating that the connection of Ru nanoparticles with abundant defects could intrinsically increase the catalytic activity towards N_2 electrochemical reduction.[39]

Given that both the adsorption of Cu adatoms and the activation of N_2 required a similar electron transfer from the electrocatalyst to the adsorbates, we further conducted the under potential deposition of Cu (Cu-UPD) to gain an in-depth understanding of the catalytic mechanism. Fig. 4c shows the Cu-UPD stripping curves of Cu adatoms on dispersed Ru nanoparticles and connected Ru nanoparticles. With the increase in oxidation potential, Cu adatoms derived from the UPD process were electrochemically oxidized. Notably, a typical peak was observed at 0.45 V *versus* RHE, which was attributed to the oxidation of Cu adatoms on the original sites of the Ru nanoparticles. In comparison with the dispersed Ru samples, a new peak arose at 0.61 V *versus* RHE in the Cu-UPD stripping curve of the connected Ru nanoparticles. This new peak could result from the oxidation of Cu adatoms on the defect sites in the connected Ru nanoparticles, which was consistent with the increase of C_{dl} values. Moreover, the location of this peak was more positive than that of the Cu stripping peaks, indicating the enhanced binding strength of the adsorbed atoms on the defect sites. This enhanced adsorption of adsorbates on the connected Ru samples further suggests the facilitated activation of N_2 during electrocatalysis.[40] The mechanism of the enhanced adsorption at the connected Ru samples was further explored using the secondary electron cut-off of the ultraviolet photoelectron spectroscopy (UPS) spectra (Fig. 4d). The work function of a catalyst is the total energy of photons in the UPS test minus the energy edge of the secondary electron cut-off. The dispersed Ru nanoparticles exhibited a work function of 4.38 eV, whereas the connected Ru nanoparticles showed a decreased work function of 4.14 eV. It has been reported that a decreased work function can improve the electron transfer process of electrocatalysts.[41–43] For the connected Ru nanoparticles, the facilitated electron transfer could benefit the faradaic process of N_2 activation, and thus lead to its enhanced performance towards N_2 electrochemical reduction.

Conclusions

In conclusion, we have developed connected Ru nanoparticles with abundant defects as highly active catalysts for the electrochemical reduction of N_2. With the existence of grain boundaries and stacking faults in the connection region of the Ru nanoparticles, the yield rate and faradaic efficiency for NH_3 production exhibited a dramatic increase. At −0.1 V *versus* RHE, the connected Ru nanoparticles exhibited a remarkable FE of 7.0%, with a considerable yield rate of NH_3 of 29.3 μg cm^{-2} h^{-1}. Moreover, the connected Ru nanoparticles showed a steady yield rate for NH_3 production during 7 h measurements. This work not only demonstrates a highly efficient electrocatalyst for N_2 electrochemical reduction but also provides an attractive strategy to design metal-based nanocrystals with well-controlled interfacial structures for catalysis and beyond.

Conflicts of interest

There are no conflicts to declare.

Acknowledgements

This work was supported by NSFC (No. 21902130) and Sichuan Science and Technology Program (No. 2020YFG0191).

Notes and references

1 C. H. Desch, *Nature*, 1922, **110**, 670–672.
2 V. Rosca, M. Duca, M. T. de Groot and M. T.-M. Koper, *Chem. Rev.*, 2009, **109**, 2209–2244.
3 X. Wei, M. Pu, Y. Jin and M. Wessling, *ACS Appl. Mater. Interfaces*, 2021, **13**, 21411–21425.
4 J. Lei, H. Liu, F. Wen, X. Jiang, C. Yuan, Q. Chen, J. Liu, X. Cui, F. Yang, W. Zhu and R. He, *Chem. Eng. J.*, 2021, **426**, 130756.
5 W. Guo, K. Zhang, Z. Liang, R. Zou and Q. Xu, *Chem. Soc. Rev.*, 2019, **48**, 5658–5716.
6 J. Wan, Y. Wang, W. Tian, H. Zhang and Y. Wang, *Appl. Surf. Sci.*, 2021, **569**, 151020.
7 J. W. Erisman, M. A. Sutton, J. Galloway, Z. Klimont and W. Winiwarter, *Nat. Geosci.*, 2008, **1**, 636–639.
8 C. J.-M. van der Ham, M. T.-M. Koper and D. G.-H. Hetterscheld, *Chem. Soc. Rev.*, 2014, **43**, 5183–5191.
9 H. Su, L. Chen, Y. Chen, R. Si, Y. Wu, X. Wu, Z. Geng, W. Zhang and J. Zeng, *Angew. Chem., Int. Ed.*, 2020, **59**, 20411–20416.

10 K. Yu, L. Tang, X. Cao, Z. Guo, Y. Zhang, N. Li, C. Dong, X. Gong, T. Chen, R. He and W. Zhu, *Adv. Funct. Mater.*, 2022, 2200315.
11 X. Yao, Z.-W. Chen, Y.-R. Wang, X.-Y. Lang, Y.-F. Zhu, W. Gao and Q. Jiang, *Appl. Surf. Sci.*, 2020, **529**, 147183.
12 Y.-C. Hao, Y. Guo, L.-W. Chen, M. Shu, X.-Y. Wang, T.-A. Bu, W.-Y. Gao, N. Zhang, X. Su, X. Feng, J.-W. Zhou, B. Wang, C.-W. Hu, A.-X. Yin, R. Si, Y.-W. Zhang and C.-H. Yan, *Nat. Catal.*, 2019, **2**, 448–456.
13 N. Cao, Z. Chen, K. Zang, J. Xu, J. Zhong, J. Luo, X. Xu and G. Zheng, *Nat. Commun.*, 2019, **10**, 2877.
14 H. Liu, J. Lei, J. Chen, Y. Li, C. Gong, S. Yang, Y. Zheng, N. Liu, Y. Liu, W. Zhu and R. He, *Nano Res.*, 2022, **15**, 2943–2951.
15 Z. Zhang, S. Qi, J. Wang and M. Zhao, *Appl. Surf. Sci.*, 2021, **563**, 150352.
16 J. Zhao and Z. Chen, *J. Am. Chem. Soc.*, 2017, **139**, 12480–12487.
17 L. Hui, Y. Xue, H. Yu, Y. Liu, Y. Fang, C. Xing, B. Huang and Y. Li, *J. Am. Chem. Soc.*, 2019, **141**, 10677–10683.
18 Y. Liu, Q. Li, X. Guo, X. Kong, J. Ke, M. Chi, Q. Li, Z. Geng and J. Zeng, *Adv. Mater.*, 2020, **32**, 1907690.
19 D. Bao, Q. Zhang, F.-L. Meng, H.-X. Zhong, M.-M. Shi, Y. Zhang, J.-M. Yan, Q. Jiang and X.-B. Zhang, *Adv. Mater.*, 2017, **29**, 1604799.
20 K. Kugler, M. Luhn, J. A. Schramm, K. Rahimi and M. Wessling, *Phys. Chem. Chem. Phys.*, 2015, **17**, 3768–3782.
21 Z. Zhang, K. Yao, L. Cong, Z. Yu, L. Qu and W. Huang, *Catal. Sci. Technol.*, 2020, **10**, 1336–1342.
22 S. Back and Y. Jung, *Phys. Chem. Chem. Phys.*, 2016, **18**, 9161–9166.
23 Z. Geng, Y. Liu, X. Kong, P. Li, K. Li, Z. Liu, J. Du, M. Shu, R. Si and J. Zeng, *Adv. Mater.*, 2018, **30**, 1803498.
24 R. Zhao, C. Liu, X. Zhang, X. Zhu, P. Wei, L. Ji, Y. Guo, S. Gao, Y. Luo, Z. Wang and X. Sun, *J. Mater. Chem. A*, 2020, **8**, 77–81.
25 A. R. Singh, B. A. Rohr, M. J. Statt, J. A. Schwalbe, M. Cargnello and J. K. Nørskov, *ACS Catal.*, 2019, **9**, 8316–8324.
26 X. F. Feng, K. L. Jiang, S. S. Fan and M. W. Kanan, *J. Am. Chem. Soc.*, 2015, **137**, 4606–4609.
27 M.-M. Shi, D. Bao, B.-R. Wulan, Y.-H. Li, Y.-F. Zhang, J.-M. Yan and Q. Jiang, *Adv. Mater.*, 2017, **29**, 1606550.
28 Y. Li, J. He, W. Cheng, H. Su, C. Li, H. Zhang, M. Liu, W. Zhou, X. Chen and Q. Liu, *Sci. China Mater.*, 2021, **64**, 2467–2476.
29 Z. Gao, D. Le, A. Khaniya, C. Dezelah, J. Woodruff, R. Kanjolia, W. Kaden, T. Rahman and P. Banerjee, *Chem. Mater.*, 2019, **31**, 1304–1317.
30 H. Liu, W. Zheng, Y. Zhao and Y. Zhou, *Anal. Chem.*, 2021, **93**, 4944–4951.
31 J. Mahmood, F. Li, S. Jung, M. Okyay, I. Ahmad, S. Kim, N. Park, H. Jeong and J. Baek, *Nat. Nanotechnol.*, 2017, **12**, 441–446.
32 Z. Wu, R. Zhang, H. Fei, R. Liu, D. Wang and X. Liu, *Appl. Surf. Sci.*, 2021, **532**, 141372.
33 Q. Jiang, Y. Meng, K. Li, Y. Wang and Z. Wu, *Appl. Surf. Sci.*, 2021, **547**, 149208.
34 S. Qi, Y. Fan, L. Zhao, W. Li and M. Zhao, *Appl. Surf. Sci.*, 2021, **536**, 147742.
35 J. Tan, X. He, F. Yin, X. Liang, G. Li and Z. Li, *Appl. Surf. Sci.*, 2021, **567**, 150801.
36 J. Gao, X. Lv, F. Wang, Y. Luo, S. Lu, G. Chen, S. Gao, B. Zhong, X. Guo and X. Sun, *J. Mater. Chem. A*, 2020, **8**, 17956–17959.
37 J. Feng and H. Pan, *J. Mater. Chem. A*, 2020, **8**, 13896–13915.
38 Y. Li, Z. Dong and L. Jiao, *Adv. Energy Mater.*, 2019, 1902104.
39 C. Li, J. Ciston and M. Kanan, *Nature*, 2014, **508**, 504–507.
40 Y. Huang, D. Babu, Z. Peng and Y. Wang, *Adv. Sci.*, 2020, 1902390.
41 H. Meng, C. Liao and M. Deng, *Angew. Chem.*, 2021, **60**(41), 22554–22561.
42 Y. Jia, L. Zhang and L. Zhuang, *Nat. Catal.*, 2019, **2**, 688–695.
43 S. Sun, R. Gao and X. Liu, *Sci. Bull.*, 2022, **67**, 389–397.